J|A|C|S
ARTICLES
Published on Web 08/18/2007

Encapsidation of Nanoparticles by *Red Clover Necrotic Mosaic Virus*

LiNa Loo,[†] Richard H. Guenther,[‡] Steven A. Lommel,[‡] and Stefan Franzen*[,†]

Contribution from the Department of Chemistry and Department of Plant Pathology, North Carolina State University, Raleigh, North Carolina 27695

Received March 18, 2007; E-mail: stefan_franzen@ncsu.edu

Abstract: Icosahedral virus capsids demonstrate a high degree of selectivity in packaging cognate nucleic acid genome components during virion assembly. The 36 nm icosahedral plant virus *Red clover necrotic mosaic virus* (RCNMV) packages its two genomic ssRNAs via a specific capsid protein (CP) genomic RNA interaction. A 20-nucleotide hairpin structure within the genomic RNA-2 hybridizes with RNA-1 to form a bimolecular complex, which is the origin of assembly (OAS) in RCNMV that selectively recruits and orients CP subunits initiating virion assembly. In this Article, an oligonucleotide mimic of the OAS sequence was attached to Au, $CoFe_2O_4$, and CdSe nanoparticles ranging from 3 to 15 nm, followed by addition of RNA-1 to form a synthetic OAS to direct the virion-like assembly by RCNMV CP. Dynamic light scattering (DLS) and transmission electron microscopy (TEM) measurements were consistent with the formation of virus-like particles (VLPs) comparable in size to native RCNMV. Attempts to encapsidate nanoparticles with diameters larger than 17 nm did not result in well-formed viral capsids. These results are consistent with the presence of a 17 nm cavity in native RCNMV. Covalent linkage of the OAS to nanoparticles directs RNA-dependent encapsidation and demonstrates that foreign cargo can be packaged into RCNMV virions. The flexibility of the RCNMV CP to encapsidate different materials, as long as it is within encapsidation constraint, is a critical factor to be considered as a drug delivery and diagnostic vehicle in biomedical applications.

Nanoparticles with useful optical and magnetic properties have been widely investigated as tools for biomedicine. The addition of biomolecules on the surface provides a method to create a multifunctional nanoparticle that is capable of cell-specific targeting and diagnostic applications. For instance, magnetic nanoparticles functionalized with tumor-targeting molecules, chlorotoxin (Cltx), are able to target a specific site for magnetic resonance imaging.[1] Quantum dots conjugated with Immunoglobulin (IgG) and streptavidin were studied to label cancer cells.[2] Gold nanoparticles conjugated with oligonucleotides were utilized as intracellular vectors for the control of protein expression.[3] The ability of protein to behave as a stabilizer or targeting vector is dependent on the organization of the protein structure on nanoparticles, which is often difficult to control. Thus, it is desirable to find alternative strategies that increase the control over surface chemistry and provide greater control based on self-assembly properties. Generally, surfactants and polymers have been used to increase particle stability and proteins have been used to provide targeting capability. For example, the poor water solubility of quantum dots is overcome by using surfactants such as mercaptoalkanoic acids[4] or encapsulation by block copolymers.[5] Synthetic polymers such as polyvinyl alcohol (PVA)[6] were also studied as a coating agent to stabilize magnetic nanoparticles. Polyethylene glycol[7] was used to prepare stable gold nanoparticle suspensions for targeting applications. Proteins such as bovine serum albumin (BSA)[8,9] and streptavidin[10] have long been used on nanoparticles to provide multiple attachment sites for targeting peptides. However, it is difficult to determine the number of proteins associated with the nanoparticle surface.

Viruses are natural protein cages with multiple functions. Their size, load capacity, structural organization, and self-assembly are desired characteristics that hold great promise for biomedical applications. Studies have demonstrated that the capsid of *Cowpea chlorotic mottle virus* (CCMV) devoid of its genome offers a constrained system that can be exploited as a container and provide protection for an encapsulated cargo.[11,12]

[†] Department of Chemistry.
[‡] Department of Plant Pathology.

(1) Veiseh, O.; Sun, C.; Gunn, J.; Kohler, N.; Gabikian, P.; Lee, D.; Bhattarai, N.; Ellenbogen, R.; Sze, R.; Hallahan, A.; Olson, J.; Zhang, M. Q. *Nano Lett.* **2005**, *5*, 1003−1008.
(2) Wu, X. Y.; Liu, H. J.; Liu, J. Q.; Haley, K. N.; Treadway, J. A.; Larson, J. P.; Ge, N. F.; Peale, F.; Bruchez, M. P. *Nat. Biotechnol.* **2003**, *21*, 452−452.
(3) Rosi, N. L.; Giljohann, D. A.; Thaxton, C. S.; Lytton-Jean, A. K. R.; Han, M. S.; Mirkin, C. A. *Science* **2006**, *312*, 1027−1030.
(4) Chan, W. C. W.; Nie, S. M. *Science* **1998**, *281*, 2016−2018.
(5) Dubertret, B.; Skourides, P.; Norris, D. J.; Noireaux, V.; Brivanlou, A. H.; Libchaber, A. *Science* **2002**, *298*, 1759−1762.
(6) D'Souza, A. J. M.; Schowen, R. L.; Topp, E. M. *J. Controlled Release* **2004**, *97*, 385−385.
(7) Latham, A. H.; Williams, M. E. *Langmuir* **2006**, *22*, 4319−4326.
(8) Tkachenko, A. G.; Xie, H.; Coleman, D.; Glomm, W.; Ryan, J.; Anderson, M. F.; Franzen, S.; Feldheim, D. L. *J. Am. Chem. Soc.* **2003**, *125*, 4700−4701.
(9) Feldherr, C.; Akin, D.; Littlewood, T.; Stewart, M. *J. Cell Sci.* **2002**, *115*, 2997−3005.
(10) Lagerholm, B. C.; Wang, M. M.; Ernst, L. A.; Ly, D. H.; Liu, H. J.; Bruchez, M. P.; Waggoner, A. S. *Nano Lett.* **2004**, *4*, 2019−2022.
(11) Douglas, T.; Young, M. *Nature* **1998**, *393*, 152−155.

Scheme 1. Schematic of Nanoparticles Encapsidation by RCNMV Coat Protein[a]

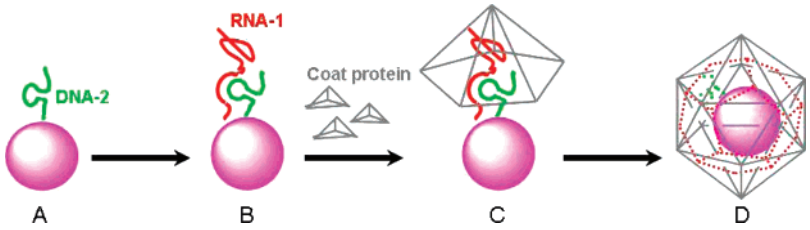

[a] (A) Conjugation of nanoparticle with DNA-2; (B) addition of RNA-1 interacts with DNA-2 to form the functional OAS; (C) the artificial OAS templates the assembly of coat protein; and (D) formation of virus-like particle with nanoparticle encapsidated.

Genetically engineered CCMV protein subunit exhibits a different charge environment inside the capsid to encapsulate a range of drugs and nanoparticles.[13] In addition, the outer surfaces of viruses present a platform that can be chemically modified to display peptides, oligonucleotides, fluorescent labels, or nanoparticles.[14−21] The attachment of artificial epitopes for antigen presentation[22] or nanoparticle magnetic resonance imaging contrast agents[23] on the virus protein surface enables it to function as a medical diagnostic tool. Furthermore, the ability of a virus to selectively target cells can be applied for diagnostic or cell-specific targeting applications. For instance, the adenoviral receptor-mediated endocytosis (RME) and nuclear localization signals (NLS) are virus-derived peptides that have been used as the most potent targeting agents.[24,25]

Red clover necrotic mosaic virus (RCNMV), a plant virus in the Dianthovirus genus, family Tombusviridae, consists of 180 identical protein subunits (37 kDa) arranged to form a $T = 3$ icosahedral virion with an outer diameter of 36 nm and an inner cavity of ~17 nm.[26] The RCNMV genome consists of two single-stranded RNAs: a 3.9 kb RNA-1, which encodes viral polymerase and capsid protein (CP), and a 1.5 kb RNA-2, which encodes the virus movement protein.[27] The RCNMV virion structure has been determined to 8 Å resolution by cryo-electron microscopy.[26] The bulk of the genomic RNA forms a $T = 1$ inner cage, with a diameter of 17 nm, within the protein capsid.[26] Like many other $T = 3$ viruses,[28] assembly of RCNMV is initiated by recognition of CP by a bimolecular RNA structure, known as the origin of assembly (OAS), which further leads to assembly of the CP into a capsid. The requirement for an RNA−RNA interaction prior to assembly of the CP provides a scaffold to create a well-characterized nanoparticle structures.

Recently, we have demonstrated a new principle for nanoparticle nanoscale self-assembly.[29] Nanoparticles were tethered with an artificial RCNMV OAS, which consists of a 20-base deoxyuridine-modified DNA oligonucleotide, which is the analogue of the RNA-2 stem loop (5′-AGAGGUAUCGCCCC-GCCUCU-3′). The sequence called DNA-2 hybridizes with full length RNA-1 to form a functional artificial OAS. The artificial OAS templates the assembly of RCNMV CP to form an enclosed protein cage (Scheme 1). The preparation of virus-like particle (VLP) with internal metallic cores is not unique to RCNMV. Since the initial report of capturing nanoparticles by self-assembly of CCMV in the presence of mineralized cores,[12] more efficient and diverse methods have been developed. Encapsulation of Au nanoparticles[30,31] and quantum dots[32] within the *Brome mosaic virus* (BMV) protein shell independent of RNA has been demonstrated. Internalization of nanoparticles in VLPs can be prepared using the capsids as natural reactors for scaffold synthesis.[33−35] The inner surface of viral capsids that formed in the absence of RNA can also be exploited as a scaffold for the synthesis of inorganic materials.[11,12] Through a pH-dependent gating mechanism, the protein shell of CCMV swells and allows molecules to diffuse into the interior cage of the virion through the opening of surface pores. The available evidence suggests that the CCMV protein shell maintains its integrity throughout the process. A more controlled assembly approach to encapsidate nanoparticles by virus protein shell was reported using synthetic DNA nucleotide sequence to mimic the high affinity capsid binding site of native RNA in BMV.[36]

Using this method, we have been able to demonstrate controlled self-assembly of the virus capsid protein around gold nanoparticles of various sizes (5−15 nm). In the present study, we further elucidated this method and extended it to magnetic nanoparticles and quantum dots. The main objective of this Article is to demonstrate that nanoparticles can be encapsidated

(12) Douglas, T.; Young, M. *Adv. Mater.* **1999**, *11*, 679.
(13) Liepold, L. O.; Revis, J.; Allen, M.; Oltrogge, L.; Young, M.; Douglas, T. *Phys. Biol.* **2005**, *2*, S166−S172.
(14) Medintz, I. L.; Sapsford, K. E.; Konnert, J. H.; Chatterji, A.; Lin, T. W.; Johnson, J. E.; Mattoussi, H. *Langmuir* **2005**, *21*, 5501−5510.
(15) Strable, E.; Johnson, J. E.; Finn, M. G. *Nano Lett.* **2004**, *4*, 1385−1389.
(16) Wang, Q.; Kaltgrad, E.; Lin, T. W.; Johnson, J. E.; Finn, M. G. *Chem. Biol.* **2002**, *9*, 805−811.
(17) Gillitzer, E.; Suci, P.; Young, M.; Douglas, T. *Small* **2006**, *2*, 962−966.
(18) Allen, M.; Bulte, J. W. M.; Liepold, L.; Basu, G.; Zywicke, H. A.; Frank, J. A.; Young, M.; Douglas, T. *Magn. Reson. Med.* **2005**, *54*, 807−812.
(19) Peabody, D. S. *J. Nanobiotechnol.* **2003**, *1*, 5−13.
(20) Khor, I. W.; Lin, T. W.; Langedijk, J. P. M.; Johnson, J. E.; Manchester, M. *J. Virol.* **2002**, *76*, 4412−4419.
(21) Lewis, J. D.; Destito, G.; Zijlstra, A.; Gonzalez, M. J.; Quigley, J. P.; Manchester, M.; Stuhlmann, H. *Nat. Med.* **2006**, *12*, 354−360.
(22) Joelson, T.; Akerblom, L.; Oxelfelt, P.; Strandberg, B.; Tomenius, K.; Morris, T. J. *J. Gen. Virol.* **1997**, *78*, 1213−1217.
(23) Anderson, E. A.; Isaacman, S.; Peabody, D. S.; Wang, E. Y.; Canary, J. W.; Kirshenbaum, K. *Nano Lett.* **2006**, *6*, 1160−1164.
(24) Tkachenko, A. G.; Xie, H.; Liu, Y. L.; Coleman, D.; Ryan, J.; Glomm, W. R.; Shipton, M. K.; Franzen, S.; Feldheim, D. L. *Bioconjugate Chem.* **2004**, *15*, 482−490.
(25) Feldherr, C. M.; Akin, D.; Cohen, R. J. *J. Cell Sci.* **2001**, *114*, 4621−4627.
(26) Sherman, M, R. H. G.; Tama, F.; Sit, T. L.; Brooks, C. L.; Mikhailov, A. M., E. V. O.; Baker, T. S.; Lommel, S. A. *J. Virol.* **2006**, *80*, 10395−10406.
(27) Basnayake, V. R.; Sit, T. L.; Lommel, S. A. *Virology* **2006**, *345*, 532−539.
(28) Tang, L.; Johnson, K. N.; Ball, L. A.; Lin, T. W.; Yeager, M.; Johnson, J. E. *Nat. Struct. Biol.* **2001**, *8*, 77−83.
(29) Loo, L.; Guenther, R. H.; Basnayake, V. R.; Lommel, S. A.; Franzen, S. *J. Am. Chem. Soc.* **2006**, *128*, 4502−4503.
(30) Dragnea, B.; Chen, C.; Kwak, E. S.; Stein, B.; Kao, C. C. *J. Am. Chem. Soc.* **2003**, *125*, 6374−6375.
(31) Sun, J.; DuFort, C.; Daniel, M. C.; Murali, A.; Chen, C.; Gopinath, K.; Stein, B.; De, M.; Rotello, V. M.; Holzenburg, A.; Kao, C. C.; Dragnea, B. *Proc. Natl. Acad. Sci. U.S.A.* **2007**, *104*, 1354−1359.
(32) Dixit, S. K.; Goicochea, N. L.; Daniel, M. C.; Murali, A.; Bronstein, L.; De, M.; Stein, B.; Rotello, V. M.; Kao, C. C.; Dragnea, B. *Nano Lett.* **2006**, *6*, 1993−1999.
(33) Knez, M.; Bittner, A. M.; Boes, F.; Wege, C.; Jeske, H.; Maiss, E.; Kern, K. *Nano Lett.* **2003**, *3*, 1079−1082.
(34) Reiss, B. D.; Mao, C. B.; Solis, D. J.; Ryan, K. S.; Thomson, T.; Belcher, A. M. *Nano Lett.* **2004**, *4*, 1127−1132.
(35) Balci, S.; Bittner, A. M.; Hahn, K.; Scheu, C.; Knez, M.; Kadri, A.; Wege, C.; Jeske, H.; Kern, K. *Electrochim. Acta* **2006**, *51*, 6251−6257.
(36) Chen, C.; Kwak, E. S.; Stein, B.; Kao, C. C.; Dragnea, B. *J. Nanosci. Nanotechnol.* **2005**, *5*, 2029−2033.

by coat protein via a RNA-dependent manner, as opposed to previous studies that utilized an RNA-independent interaction for encapsulation of nanoparticles.

Materials and Methods

Nanoparticles and Quantum Dots. 5, 10, 15, and 20 nm Au nanoparticles were purchased from Ted Pella Inc. Bis(*p*-sulfonatophenyl)phenylphosphine dihydrate (BSPP) was used as received from Strem Chemicals. Reagents to synthesize cobalt iron oxide, $CoFe_2O_4$ nanoparticles, which included $CoCl_2 \cdot 6H_2O$, $FeCl_2 \cdot 4H_2O$, and methylamine, were obtained from Aldrich. Mercaptopropionic acid coated-quantum dots (MPA-Qds) was received as a gift from Applied Biosystem, Inc. ~1 mg of Qds was dissolved in a 1 mL solution of 4-(dimethylaminopyridine) (DMAP) in *N*,*N*-dimethylformamide (DMF) (20 mg of DMAP in 1 mL of DMF). The preparation of RCNMV CP and transcript RNA-1 was as described previously.[29]

***In Vitro* Assembly of RCNMV Capsid Protein (CP).** 20 μL of RCNMV CP (0.5 mg/mL) was brought up to a total volume of 100 μL with glycine-NaOH, pH 10. For the analysis of the pH effect on *in vitro* assembly, the RCNMV CP solution is dialyzed, using a Slide-A-Lyzer Dialysis Cassette (10 kDa molecular weight cutoff) against 50 mM Tris buffer at three different pH's (5.5, 6.0, and 6.5) for overnight at room temperature. The assembled VLPs formed at each pH are collected and analyzed by DLS.

Preparation of DNA Conjugated Nanoparticles. The 5′-thiol deoxyuridine-modified DNA oligonucleotide, DNA-2, with the sequence SH-5′-AGAGGUAUCGCCCCGCCUCU-3′ was synthesized by MWG Biotech. To deprotect the thiol group, 1 mL of a 100 mM solution of dithiothreitol (DTT) was added to the DNA-2. This mixture was allowed to react for 30 min at room temperature. Excess DTT was removed using a Micro Bio-Spin P-30 purchased from Biorad.

DNA: Au Conjugates. Au nanoparticles coated with BSPP were synthesized as described.[37] A 1:300 mole ratio of Au nanoparticles to DNA-2 was incubated at 37 °C for 8 h in 100 μL of 10 mM phosphate buffer, pH 7. The mixture was then brought up to 500 μL with 0.1 M NaCl/10 mM phosphate buffer, pH 7, and incubated for an additional 40 h. Unattached DNA was removed by centrifugation at 14 000 rpm for 25 min. The supernatant, which consists of the unreacted DNA, was removed followed by dispersed of the precipitation in 500 μL of 10 mM phosphate buffer, pH 7, and recentrifuged. This step was repeated twice. The DNA/Au conjugates were then resuspended in 10 mM phosphate buffer, pH 7.

DNA: $CoFe_2O_4$ Synthesis and Conjugation. $CoFe_2O_4$ nanoparticles with mean sizes of 4, 10, and 15 nm were synthesized as described.[38] Transmission electron microscopy (TEM) and dynamic light scattering (DLS) analysis of the nanoparticles confirmed a size variation of <30% in each batch. 10 mg of $CoFe_2O_4$ nanoparticles was added with 50 μL of DNA-2 (96 μM). The solution was allowed to stir overnight at room temperature. DNA/$CoFe_2O_4$ conjugates were collected with a magnetic bar and washed with 50% ethanol three times to remove unreacted DNA-2.

DNA: Quantum Dot Conjugates. Mercaptopropionic acid coated-quantum dots (MPA-Qds) were combined with DNA-2 in a mole ratio of 1:40. The mixture was incubated in 37 °C water bath for 12 h. The solution was brought up to 500 μL with 0.1 M NaCl/10 mM phosphate buffer, pH 7, and incubated at 37 °C for an additional 12 h. Unreacted DNA-2 was removed by passing the reaction mixture through a Microcon YM30 membrane.[39]

Encapsidation of Nanoparticles into VLPs. The nanoparticle encapsidation protocol by RCNMV CP was as conducted essentially as described previously.[29] DNA/nanoparticle conjugates were added with 1 μL of T7 RCNMV RNA-1 transcripts (4 mg/mL). This mixture was allowed to incubate for 10 min, followed by the addition of 5 μL of purified RCNMV CP (10 mg/mL) harvested from wild-type virions reared in *Nicotiana clevelandii* plants. Encapsidation reactions were carried out by dialyzing the sample against 50 mM Tris-HCl, pH 5.5, overnight at room temperature, using a Slide-A-Lyzer Dialysis Cassette (10 kDa molecular weight cutoff). VLPs encapsidated nanoparticles were isolated by ultra centrifugation through a sucrose cushion at 218 000*g* for 20 min in a SW-55 rotor with a model L8-70 Beckman ultracentrifuge.

Table 1. DLS Measurement of the Mean Hydrodynamic Diameter (D_H) of Empty VLPs Formed at Various pH Values

pH	mean hydrodynamic diameter (D_H), nm
5.5	29.8 ± 3.0
6.0	45.6 ± 2.0
6.5	48.5 ± 2.3, 73.1 ± 2.0

Optical Characterization of VLPs Encapsidated Nanoparticle. UV−vis absorption spectra were carried out on an Hewlett-Packard HP8453 diode array absorption spectrophotometer. TEM images were acquired using a (Philips) CM12 electron microscope operating at 100 kV accelerating voltage located at University of North Carolina, School of Dentistry, Chapel Hill, NC. Images were created with a Gatan 780 DualView camera system. All TEM samples, unless otherwise noted, were negatively stained with 2% uranyl acetate to enhance image contrast. Samples were prepared by placing 10 μL of VLPs encapsidated nanoparticles solution onto a carbon-coated grid and stained with 2% uranyl acetate. Excess liquid was blotted, and the grid was allowed to dry. Digital micrograph software was used to measure the diameters of the virus-like particles and inner cores from the TEM images. High-resolution TEM and electron diffraction pattern images were recorded with a JEOL 2010F TEM, operating at 200 kV accelerating voltage from the Department of Materials Science and Engineering, North Carolina State University. DLS data were collected on a Malvern Zetasizer 1000HS spectrometer. The scattering data were best fit using the Contin algorithm.

Results

Characterization of the *in Vitro* Assembly of RCNMV Capsid Protein (CP). The *in vitro* assembly properties of the CP were investigated to determine the suitability of RCNMV CP to encapsidate nanoparticles. The reassembly of CP isolated from RCNMV virions in the absence of genomic RNA was determined at pH's 5.5, 6.0, and 6.5. These capsids devoid of RNA are considered empty capsids. The apparent diameter of the empty capsids measured using DLS at three pH values is given in Table 1. Comparing the diameter of particles formed under these pH's, empty particles formed at pH 5.5 were observed to have the diameter closest to the native RCNMV. Further analysis by TEM indicated that VLP devoid of the virus genome formed at this pH was observed to have different morphologies[29] and was unable to withstand centrifugation. From these data, we conclude (1) that pH 5.5 is chosen for subsequent encapsidation experiments, because this pH yields particle with the diameter closest to that of the native RCNMV, and (2) VLPs devoid of the virus genome have a diameter of ~30 nm with a different morphology. The formation of smaller than native VLP was also shown for *Southern bean mosaic virus*[40] where the CP was found to form $T = 1$ particles when placed in favorable conditions in the absence of viral RNA.

(37) Loweth, C. J.; Caldwell, W. B.; Peng, X. G.; Alivisatos, A. P.; Schultz, P. G. *Angew. Chem., Int. Ed.* **1999**, *38*, 1808−1812.
(38) Rondinone, A. J.; Samia, A. C. S.; Zhang, Z. J. *J. Phys. Chem. B* **2000**, *104*, 7919−7922.
(39) Mitchell, G. P.; Mirkin, C. A.; Letsinger, R. L. *J. Am. Chem. Soc.* **1999**, *121*, 8122−8123.
(40) Erickson, J. W.; Silva, A. M.; Murthy, M. R. N.; Fita, I.; Rossmann, M. G. *Science* **1985**, *229*, 625−629.

Table 2. Experimental and Theoretical Melting Temperature, T_m (°C), of DNA-2 (20-mer) at Three Different Concentrations

concentrations of DNA (μM)	melting temperature, T_m (°C)		
		theoretical	
	experimental	duplex[42]	hairpin[44]
0.2	43.5 ± 0.5	−6.5	43.5
2	45.2 ± 0.7	1.5	43.5
16	43.9 ± 0.6	9.1	43.5

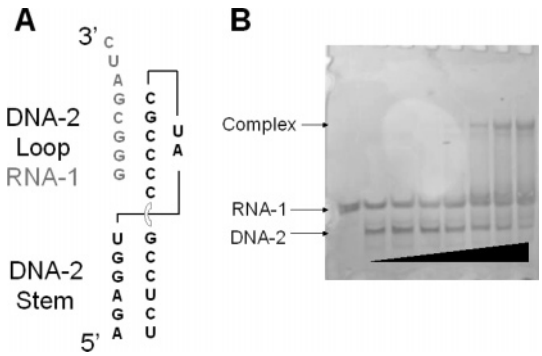

Figure 1. (A) The sequences of DNA-2 and RNA-1 are depicted in the kissing loop complex that comprises a model for the OAS. (B) Gel shift assay to measure the binding constant for interaction of the DNA-2 (20-mer) with the RNA-1 (8-mer oligonucleotide).

Characterization of the *in Vitro* Properties of the Synthetic OAS Element. The synthetic DNA-2 must hybridize with RNA-1 to function as a synthetic OAS. The OAS of RCNMV was comprised of two regions of the viral genome that interact to form a pseudoknot-like structural complex.[41] Two experiments were performed to determine whether DNA-2 forms a similar complex. First, the thermodynamic properties of the synthetic DNA-2 were determined by UV monitored thermal denaturation. Analysis of the thermodynamic parameters reveals that the synthetic DNA-2 contains two stable conformations (Table 2). The duplex form is observed in the millimolar range of DNA-2 concentration, particularly at high NaCl concentration. However, the hairpin conformation has the largest population at low concentration. Thus, hairpin formation is dominant at the low concentration (nM) of DNA-2 used in the encapsidation experiment. The observed melt temperatures, T_m, are consistent with the existence of a hairpin as the dominant form (Table 2). The table also includes the theoretical T_m values for both the duplex and the hairpin.[42] Duplex formation was observed in NMR spectra and UV melt profiles at millimolar and micromolar concentrations of DNA-2, respectively (data not shown).

The ability of the synthetic DNA-2 to bind to RNA-1, as shown in Figure 1A, was studied by a band shift assay. It has previously been shown that the native OAS was comprised of a bimolecular complex RNA-2 with short oligonucleotide analogues of RNA-1 *in vitro*.[43] The interaction of DNA-2 (20-mer) with RNA-1 (8-mer oligonucleotide) was observed using a band shift assay shown in Figure 1B. The apparent association constant was similar for both the artificial OAS (DNA-2/RNA-1) and the native OAS (RNA-2/RNA-1).[41]

(41) Guenther, R. H.; Sit, T. L.; Gracz, H. S.; Dolan, M. A.; Townsend, H. L.; Liu, G. H.; Newman, W. H.; Agris, P. F.; Lommel, S. A. *Nucleic Acids Res.* **2004**, *32*, 2819−2828.
(42) Markham, N. O.; Parry, E. M.; Stefanovic, M.; Gallagher, P. G.; Low, P. S.; Bodine, D. M. *Blood* **2005**, *106*, 473A−474A.
(43) Sit, T. L.; Vaewhongs, A. A.; Lommel, S. A. *Science* **1998**, *281*, 829−832.

Table 3. Effect of Encapsidated Nanoparticle Diameter on the Inner and Outer Diameters of VLP As Measured by TEM

nanoparticle diameter (nm)	VLP outer diameter (nm)	VLP inner diameter (nm)
Au (5.0 ± 0.5 nm)	30.0 ± 3.0	6.0 ± 0.5
Au (10.0 ± 1.0 nm)	33.5 ± 3.0	10.0 ± 2.0
Au (15.0 ± 1.5 nm)	34.0 ± 2.0	15.0 ± 2.0
$CoFe_2O_4$ (4.0 ± 1.2 nm)	33.1 ± 2.2	4.0 ± 0.5
$CoFe_2O_4$ (10.0 ± 3.0 nm)	34.2 ± 1.4	9.8 ± 1.1
$CoFe_2O_4$ (15.0 ± 4.5 nm)	34.0 ± 2.0	15.0 ± 2.0
quantum dots (4.0 ± 1.0 nm)	31.6 ± 3.3	4.0 ± 1.5

Encapsidation of 5, 10, and 15 nm Au Nanoparticles. Given that RCNMV CP will self-assemble to produce different sizes and morphologies of VLPs under a range of conditions, experiments were performed to determine if nanoparticles would act as nucleating cores for CP self-assembly. Encapsidation of 5, 10, and 15 nm of Au conjugated with oligonucleotide DNA-2, analogue of the RNA-2 of OAS, has been described previously.[29] After VLPs were purified through a 50% sucrose cushion centrifugation, TEM images showed VLPs consist of closed protein shell, with an electron dense inner core.[29] The purified VLPs were homogeneous in size with an average diameter of 33.5 ± 3.0 nm (15−25 VLPs per grid square), 30.0 ± 3.0 nm (5−10 VLPs per grid square), and 34.0 ± 2.0 nm (30−50 VLPs per grid square), for encapsidation of 5, 10, and 15 nm Au, respectively. The average sizes of the electron dense VLPs inner cores were consistent with the size of Au nanoparticles used in these encapsidation experiments (Table 3). The attempt to encapsidate a 20 nm Au nanoparticle yielded no VLPs even before the purification procedure was employed. The lack of assembly around a 20 nm particle is consistent with an upper packaging constraint equaling the 17 nm cavity in wild-type virions. The failure to encapsidate a 20 nm Au nanoparticle provides additional evidence that 5, 10, and 15 nm Au nanoparticles were in fact encapsidated within RCNMV CP, because nonspecific coating of a nanoparticle by CP does not rely on the size of Au nanoparticle.

The 50% sucrose cushion required to concentrate the VLPs encapsidated Au, as compared to the 20% sucrose utilized in native virion purification, indicated the significant structural robustness of the VLPs. To further determine the difference in density, VLPs encapsidated Au was subjected to 20−50% sucrose gradient centrifugation. The VLP encapsidated Au was observed to sediment at lower band (heavier density) than the native RCNMV (Supporting Information). The absorbance profile on fractionated sucrose gradient indicated that the highest value of absorbance for both protein (A_{280nm}) and Au (A_{520nm}) of VLP encapsidated Au was at fraction 1, equivalent to 50% sucrose. In comparison, native RCNMV was detected at fraction 8, which corresponded to 20% sucrose. Based on the refractive index measurements, the density of VLP encapsidated Au was 1.2299 g/mL, as compared to native RCNMV, which was 1.1368 g/mL.

The VLP encapsidated Au was subjected to a 2% agarose gel electrophoresis. When compared to DNA-modified Au and unmodified Au, a significant reduction in mobility was observed for Au after CP packaging, providing physical evidence of VLPs formation. Absorbance measurements showed that the plasmon resonance of encapsidated Au shifted to 530 nm as compared to 520 nm of Au before encapsidation (see Supporting Information). The red-shift of plasmon resonance was probably due to

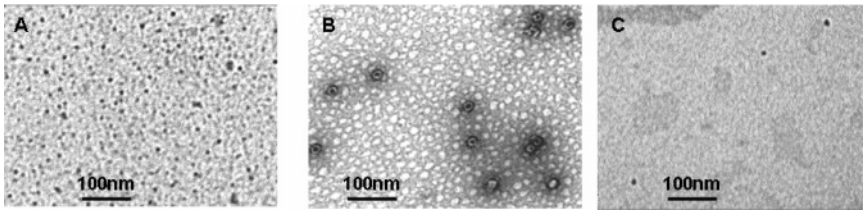

Figure 2. TEM images of (A) 4 nm $CoFe_2O_4$ nanoparticles, (B) negatively stained sample of VLP encapsidated 4 nm $CoFe_2O_4$ nanoparticles prior to purification, and (C) unstained sample of VLP encapsidated 4 nm $CoFe_2O_4$ nanoparticles after purification.

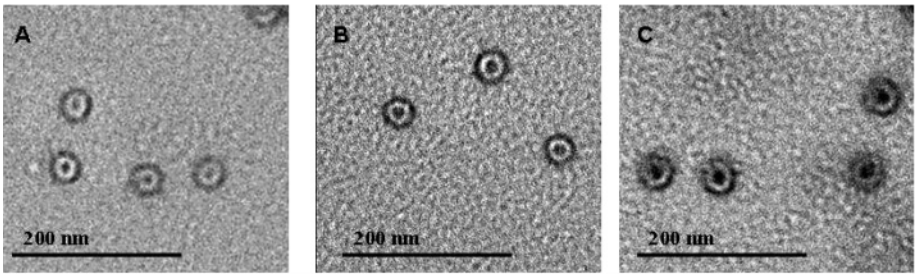

Figure 3. Negatively stained TEM images of VLP encapsidated (D) 4 nm $CoFe_2O_4$, (E) 10 nm $CoFe_2O_4$, and (F) 15 nm $CoFe_2O_4$ nanoparticles after purification.

the increase of the refractive index in response to the protein layer.[45] Preliminary studies to characterize the encapsidated Au by selected area electron diffraction revealed that the characteristic rings matched with the known reflecting planes of fcc Au. Moreover, analyses by HR-TEM indicated that lattice fringes were observed on Au encapsidated by VLP. The combination of electron diffraction and HR-TEM analyses indicated the composition of Au remained even after encapsidation by VLP.

The OAS attachment to Au nanoparticles was also characterized. VLP encapsidated Au nanoparticles were exposed to pH > 9 to induce structural disruption. Phenol extraction was performed to precipitate RNA-1. Based on the measured absorbance, the ratio of RNA-1 to Au nanoparticle was determined to be 1:1 using the UV−vis extinction coefficient (data not shown). This ratio is also consistent with the observed ratio of RNA-1 to CP. The A_{260}/A_{280} ratio of native RCNMV is 1.6. Based on the absorbance measurement, the ratio of DNA/RNA (A_{260}) to protein (A_{280}) of VLP is 1.43, which is approximately 10% lower than native virus as expected because the VLP consists of native RNA-1 (3.9 kb) and DNA-2, which is a sequence of only 20 nucleotides in place of native RNA-2, which is 1.5 kb.

Control experiments were performed that included encapsidation of Au-coated BSPP (in the absence of OAS), a random DNA sequence to replace DNA-2, and a random ssRNA sequence to replace RNA-1. No VLPs were observed after purification. This control experiment validates the requirement of the OAS for nanoparticle encapsidation and VLPs assembly.[29]

Encapsidation of 4, 10, and 15 nm $CoFe_2O_4$ Nanoparticles. To further study the versatility of RCNMV CP as an agent for encapsidation, the methods described above were applied to 4, 10, and 15 nm $CoFe_2O_4$ nanoparticles. Prior to VLP purification, TEM images indicated the presence of VLPs encapsidated $CoFe_2O_4$ nanoparticles, empty VLPs, minor aggregation of $CoFe_2O_4$ nanoparticles, as well as failed products ($CoFe_2O_4$ nanoparticles that were not fully covered by CP) (Figure 2B). Following the initial mixing, the sample was collected and concentrated using a magnetic bar to separate VLPs encapsidated $CoFe_2O_4$ nanoparticles from excess CP and empty VLPs. The sample was further purified through a 30% sucrose cushion by ultra-centrifugation to remove aggregated $CoFe_2O_4$ nanoparticle and other failed products. Figure 3 shows TEM images of VLPs encapsidated $CoFe_2O_4$ purified by magnetic concentration and centrifugation. A negative stain of the sample showed the presence of the intact protein shell encapsidated $CoFe_2O_4$ nanoparticles. Encapsidation of 4, 10, and 15 nm $CoFe_2O_4$ nanoparticles yields 33.1 ± 2.2 nm (8−20 VLPs per grid square), 34.2 ± 1.4 nm (9−13 VLPs per grid square), and 34.0 ± 2.0 nm (40−55 VLPs per grid square) diameter VLPs, respectively. In an unstained sample, the measured inner cores were observed to be consistent with the diameter of the $CoFe_2O_4$ nanoparticles used in the assembly procedure (Table 3). The attempts to encapsidate nanoparticles >15 nm in diameter led to the formation of unstable particles that did not withstand purification by sucrose cushion centrifugation, which is consistent with the results obtained when the encapsidation experiment was performed on 20 nm Au nanoparticles.

Characterization of encapsidated $CoFe_2O_4$ performed by XPS indicated that the spectra for Co 2p and Fe 2p of $CoFe_2O_4$ nanoparticles before and after encapsidation by VLP showed a similar group of peaks (Supporting Information). The Co $2p_{3/2}$ peak from $CoFe_2O_4$ encapsidated by VLP (binding energy of 772.49 eV) was observed to match the binding energy of Co $2p_{3/2}$ for $CoFe_2O_4$ nanoparticles before encapsidation. A similar observation was also reported for Fe 2p, where the peak that corresponded to Fe $2p_{3/2}$ (binding energy of 704.89 eV) for $CoFe_2O_4$ nanoparticles before encapsidation coincided with Fe $2p_{3/2}$ for $CoFe_2O_4$ encapsidated by VLP.

DLS analysis of VLPs encapsidated 10 nm $CoFe_2O_4$ nanoparticles indicated that VLP exhibited pH-dependent swelling comparable to native RCNMV (Figure 4A). When exposed to pH 8, the diameter of VLPs increased from 33.5 ± 3.0 to 54.2 ± 3.0 nm. At pH > 9, VLPs disassembled to release the encapsidated $CoFe_2O_4$ nanoparticles as indicated in Figure 4B. The lower peak (11.3 nm) corresponds to $CoFe_2O_4$ nanopar-

(44) Dimitrov, R. A.; Zuker, M. *Biophys. J.* **2004**, *87*, 215−226.
(45) Henglein, A.; Mulvaney, P.; Linnert, T. *Faraday Discuss.* **1991**, 31−44.

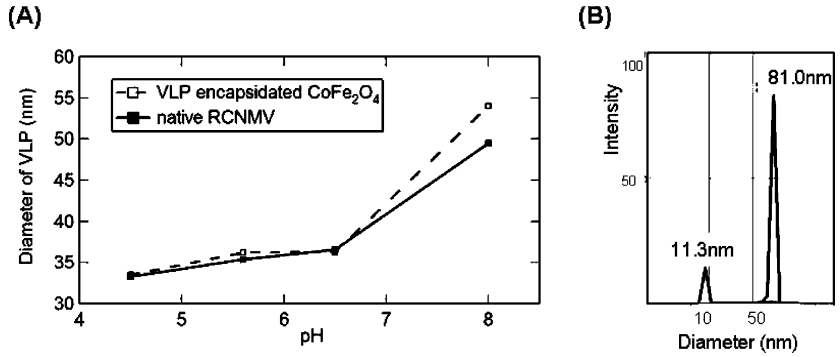

Figure 4. (A) Hydrodynamic radius of native RCNMV and VLP encapsidated 10 nm $CoFe_2O_4$ in the range of pH 4.5−8 as determined by DLS. (B) DLS of VLP encapsidated 10 nm $CoFe_2O_4$ at pH > 9. Structural disruption of VLP indicated the release of encapsidated $CoFe_2O_4$ nanoparticles.

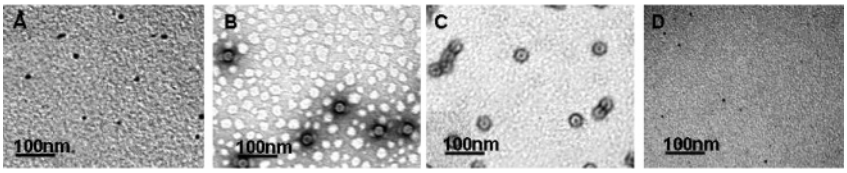

Figure 5. TEM images of (A) 4 nm quantum dots, (B) negatively stained sample of VLP encapsidated quantum dots prior to purification, (C) negatively stained sample of VLP encapsidated quantum dots after purification, and (D) unstained sample of VLP encapsidated quantum dots after purification.

ticles, while the higher peak (81.0 nm) indicated the disrupted VLPs. These data also support the hypothesis that the $CoFe_2O_4$ nanoparticles were encapsidated within CP and not attached on the outer surface of the protein. If nanoparticles were attached on the outer protein shell, high pH VLP disruption would result in a single peak with the nanoparticles remaining attached on disrupted CP.

Encapsidation of Quantum Dots (Qds). Encapsidation of quantum dots was carried out using procedures similar to those described above. Analysis of TEM images before purification indicated a large amount of empty particles and distorted VLP (Figure 5B). After purification by centrifugation through a 50% sucrose cushion, these empty particles and distorted VLPs were not observed. When an identical sample was negatively stained, the protein cage remained intact and surrounded the interior core (Figure 5C). The VLPs (5−15 VLPs per grid square) were found to be homogeneous in size with an average diameter of 31.6 ± 3.3 nm and an electron-dense core with an average diameter of 4 nm, commensurate in size with the quantum dots. The remaining VLPs after isolation process indicated the high stability of the encapsidation of quantum dots by RCNMV CP. Preliminary studies on encapsidated Qds were performed on the basis of fluorescence measurements. The emission wavelength of Qds encapsidated by VLP appeared to be shifted 1−2 nm as compared to the Qds before encapsidation (Supporting Information). This result is consistent with the observation reported for Qds packaged by BMV where a shift of emission wavelength was also detected.[32]

Discussion

The present study demonstrates a novel method that utilizes the RCNMV OAS to direct self-assembly of virus CP that leads to encapsidation of nanoparticles within the protein shell. A functional 20-nucleotide deoxyuridine-modified DNA analogue of the RNA-2 of OAS is attached to a nanoparticle and then base-paired through an 8-nucleotide complementary sequence in genomic RNA-1 (3.9 kb total length) to form the functional OAS. Nanoparticles presenting the OAS can nucleate the self-assembly of the capsid protein. The requirement of these elements for VLP formation is similar to the elements for native RNA-dependent encapsidation of RCNMV. This method yields uniform sized of VLP, independent of the composites and sizes of cores used in this Article. The average diameter of the VLP formed from the seven different cores tested, 32.8 nm, was less than that of the native virus at 36.6 nm. Attempts to encapsidate nanoparticles with diameters larger than 17 nm failed to yield well-formed VLPs. In other words, the critical limit for encapsidation of nanoparticles is <17 nm. This observation is expected as structural studies indicate the inner cavity of the virus to be approximately 17 nm in diameter.[26]

A common aspect in the *in vitro* self-assembly of icosahedral plant viruses is the use of pH to facilitate capsomere assembly.[46,47] A pH reduction likely ionizes the many charged residues characteristic of CP, resulting in protein−protein and RNA−protein interactions that promote capsid assembly to form native-like particles.[48] For BMV, the balance of electrostatic charges can be achieved for the VLP encapsidation by coating the surface of nanoparticles by DNA or PEG.[31,36] For RCNMV, the requirement for encapsidation of a nanoparticle to form VLP is dependent on the presence of two critical components: the OAS and a nucleating core of appropriate size. The absence of either one of these components either prevented formation of VLPs or generated VLPs that were significantly smaller than the native virion. The requirement for RNA to form stable VLP for *Tombusviridae* suggested a different self-assembly mechanism may be involved as compared to bromoviridae.

The self-assembly design process and VLP formed in the present study may have advantages over other approaches. The requirement for a synthetic DNA element and an RNA scaffold affords a unique kind of control over the assembly process. This approach to VLP preparation is a straightforward method that can be applied to a wide range of starting materials, with an

(46) Ren, Y. P.; Wong, S. M.; Lim, L. Y. *J. Gen. Virol.* **2006**, *87*, 2749−2754.
(47) Phelps, J. P.; Dao, P.; Jin, H. F.; Rasochova, L. *J. Biotechnol.* **2007**, *128*, 290−296.
(48) Fox, J. *Virology* **1998**, *244*, 212−218.

array of useful properties, to produce a uniform product. The sizes of VLP produced are significantly smaller than those reported for most other non-viral nanoparticle approaches.[49] While it is unclear if there is an optimal size for diagnostic and therapeutic nanoparticles, a VLP in the 30 nm range is small enough to be delivered directly to the nucleus of mammalian cells by passing through the nuclear membrane pores. An additional advantage of this method is the ability of the particles to withstand magnetic or centrifugation purification, which demonstrates a structural integrity that is necessary to obtain usable quantities of material for any biomedical application. This protein surface of this VLP can also serve as a platform for peptide-conjugation, which further enhances the functionality of the particle. The VLPs obtained by the method reported here have advantages that can address problems associated with the use of nanoparticles in biomedical applications.

Acknowledgment. S.F. acknowledges support through NIH grant NCI CA098194. We would like to thank Applied Biosystems, Inc., for providing the quantum dots used in this study. We thank Dr. Wallace Ambrose in the School of Dentistry at UNC for help with TEM and Dr. Tim Sit for help with the RCNMV molecular biology. We thank Dr. Gerd Josef-Manfred Dusher for help with HR-TEM and electron diffraction of Au.

Supporting Information Available: Supplementary figures. This material is available free of charge via the Internet at http://pubs.acs.org.

JA071896B

(49) Oberdorster, G.; Oberdorster, E.; Oberdorster, J. *Environ. Health Perspect.* **2005**, *113*, 823−839.